SCIENCE CHINA
Chemistry

• ARTICLES •

September 2011 Vol.54 No.9: 1461–1467
doi: 10.1007/s11426-011-4316-9

Synthesis and shape memory behavior study of hyperbranched poly(urethane-tetrazole)

QIAO LiGen[1], ASIF Anila[2] & SHI WenFang[1*]

[1]CAS Key Laboratory of Soft Matter Chemistry, Department of Polymer Science and Engineering, University of Science and Technology of China, Hefei 230026, China
[2]Interdisciplinary Research Centre in Biomedical Materials, COMSATS Institute of Information Technology, Defence Road, Off Raiwind Road, Lahore 54000, Pakistan

Received March 20, 2011; accepted April 13, 2011; published online June 11, 2011

A novel hyperbranched poly(urethane-tetrazole) (HPUTZ) was synthesized via the “A_2+BB'_2” approach using hexadiisocyanate (HDI) and 3-(bis-(2-hydroxyethyl)) aminopropyltetrazole (HAPTZ). The molecular structure was characterized by FTIR and ^{1}H NMR spectroscopy. The number average molecular weight was measured to be 1.05×10^4 g/mol with a polydispersity of 1.27 by GPC analysis. The HPUTZ was further cured by the semi-adduct (PEG-IPDI) from polyethylene glycol (PEG) reacting with isophorone diisocyanate (IPDI) to form the crosslinked HAPTZ-PU film in different ratio of HAPTZ to PEG-IPDI. The glass transition temperature of HAPTZ-PU increased from 44.9 to 56.4 °C as the HPUTZ content increased from 20% to 33% from the DSC analysis. The DMA results indicated that the HPUTZ-PU with 20% HPUTZ possessed the highest storage modulus and loss tangent. However, the storage modulus increased with the increasing of HPUTZ segment at higher temperature. The shape memory study showed that all the films presented the excellent shape memory function. Over 98% shape recovery could be obtained for the HAPTZ-PU with 20%–33% HAPTZ segment content within 60 s in the tension deformation test and within 40 s at 80 °C in the bend deformation test.

synthesis, hyperbranched poly(urethane-tetrazole), shape memory behavior, thermal property

1 Introduction

The conceptual category of smart materials has been extended to various application fields, such as sensors, medical, electronic, and so on [1, 2]. In recent years, the shape memory polymers (SMPs) have been proposed as a group of smart materials. Their temporary or permanent deformation can be eliminated at a critical temperature. The SMPs possess some significant advantages such as lightweight, larger recoverable deformation, lower manufacturing cost and lower recovery temperature compared to traditional shape memory alloys. Therefore, the expected industrial applications have been made for such as heat-shrinkable materials, self-healing coatings, and packaging materials [3].

The shape memory polyurethanes (SMPUs) were widely studied due to their excellent shape memory behavior. The micro-phase separated structure of SMPU was generated by a frozen phase and a reversible phase. The presence of strong hydrogen bonding in SMPU plays a key role in forming the stable frozen phase. Whereas, the reversible phase usually consists of soft segments such as long alkyl chain, and mainly for providing the shape memory performance. Because two phases are connected by chemical bonds, the phase-separation is limited naturally, and endows SMPU showing the circular shape memory property [4–9]. Moreover, the shape recovery behavior of SMPU can be adjusted in a large temperature range by controlling the hard segment content in the polymer chain. Hence, SMPU materials are designed to prepare various products with different storage modulus which affects the shape memory function such as shape-fixed length and shape recovery rate [10, 11].

---

*Corresponding author (email: wfshi@ustc.edu)

However, the SMPU materials were recently developed mainly as linear polymers or block copolymers [12–14]. Little was investigated with hyperbranched polymers used as shape memory materials. Liu and his coworkers synthesized a series of polyurethanes upon the hyperbranched polyester, Boltorn^{TM} H30 [15]. The poly(butyleneadipate)glycol 2000 terminated with methylenediphenyl diisocyanate was used to cure with the hyperbranched polyester at high temperature. They have observed that the cured films possessed the excellent shape memory properties due to the presence of abundant hydrogen bonding which affects the micro-phase separated structure. Sivakumar and his coworkers prepared a series of hyperbranched polyurethanes with different molecular weights via the $A_2 + B_3$ approach [16].

The tetrazole compounds possessing a five-membered aromatic heterocycle with four N atoms on the ring have been widely used in organic chemistry, coordination chemistry, and especially biomedical science [17, 18]. The tatrezole is shown as a kind of acid (pKa (tetrazole) = 4.89, while pKa (acetic acid) = 4.75) [19], but undergoes longer metabolic degradation than a carboxylic acid, which results in that the tetrazole is a suitable choice instead of carboxylic acid for biomedical science. Dozens of linear polymers containing tetrazole group were synthesized in previous studies [19–21]. The poly-1-vinyl-5-aminotetrazole and poly (glycidyl methacrylate) containing 5-aminotetrazole were prepared for different application purposes [20, 21]. Due to the proton transport between hydrogen bonds of neighboring heterocyclic units through structure diffusion, the stable dispersed domains that act as physical crosslinkers (frozen phase) via the strong hydrogen bonding in a polymer containing tetrazole group are expected to form. However, to the best of our knowledge, the hyperbranched polymers containing both urethane and tetrazole segments have never been prepared for shape memory material applications before.

In this study, the hyperbranched poly(urethane-tetrazole) (HPUTZ) via the “A_2+BB'_2” approach based on the PEG soft segment and the hyperbranched poly(urethane-tetrazole) (HPUTZ) hard segment was prepared. The shape memory behavior was examined extensively. The linear polymer with the similar structure as that of HPUTZ-PU was not synthesized in this work. However, from the chemical structure of hyperbranched copolymer HPUTZ-PU, it can be found that compared to linear copolymers, the synthesized copolymers supply much more extensive hydrogen bond structures, which directly affect the micro-phase separated structure. And the content and distributing of hard and soft segments play a key role in the shape recovery property of films.

2 Experimental

2.1 Materials

Sodium azide (NaN_3) was supplied by Aldrich and used as received. All other chemicals were supplied by First Reagent Co. of Shanghai, China. Diethanolamine (DEA), acrylonitrile (AN), isophorone diissocyanate (IPDI) and hexadiisocyanate (HDI) were used after distillation, and the solvents were dried before use.

2.2 Measurements

The ^{1}H NMR spectra were recorded with an AVANCE 300 Bruker spectrometer using tetramethylsilane as an internal reference and $CDCl_3$, D_2O and DMSO-d_6 as solvents.

The FTIR spectra were recorded using a Nicoler MAGNA-IR 750 spectrometer with a KBr disk.

The molecular weight and its distribution were determined by a waters gel permeation chromatography (GPC) system with a refractive index detector using DMF as an eluent and polystyrene as a standard polymer for calibration.

A Pyris Diamond DMS 6100 instrument (Perkin-Elmer Co., USA) was used to measure the storage modulus and Tanδ at an oscillation frequency of 1 Hz with an astatic force of 10 mN. The running temperature was set in the range of –40 to 120 °C at a heating rate of 10 °C/min under nitrogen atmosphere. The crosslinking density of curing films v_e is defined as the mole number of effective elastic chains per cubic centimeter and calculated by the DMA results from the following equation $v_e = E'/3RT$, where E' is the storage modulus, R is the gas constant, T is the kelvin temperature. E' can be obtained from the DMA results in the rubber state. Because different composition ratios were used, the curing films possessed various crosslinking densities from their mechanical properties.

The DSC curves were recorded using a Perkin-Elmer Diamond differential scanning calorimeter (DSC) with a heating rate of 10 °C/min from 20 to 100 °C, and then cooled to 20 °C at a cooling rate of 200 °C/min, followed by a second scan at the same heating rate to 100 °C, and calibrated with a base line.

The shape memory behavior of HPUTZ-PU was examined using the tension deformation test. The size of 0.8 mm (thickness) × 30 mm (width) × 10 mm (length) for all samples was used in the tests. The sample was first stretched to the elongation of 250% at 80 °C, and then cooled quickly at 0 °C and kept for 5 min in order to fix the deformation. The fixed length of the deformed sample was measured. The deformation length and shape recovery properties were recorded in a water bath at different temperatures during the shape recovery course. The shape fixity (F_s) and shape recoverability of a film (R_s) are defined as follows [15]:

$$F_s = (L_F–L_o)/(L_{max}–L_o)\times 100\% \tag{1}$$

$$R_s = (L_F–L_t)/(L_F–L_o)\times 100\% \tag{2}$$

Where L_o is the original length, L_F is the fixed length at 0 °C, L_{max} is the maximum stretched length (at the elongation of 250%), and L_t is the length in the course of shape recovery at time.

For recording the shape recovery course, the sample size of 0.5 mm (thickness) × 30 mm (width) × 10 mm (length) was used in the bend deformation test. The film was firstly bent to a circular shape with a diameter of 9.55 mm at 80 °C by a water bath under an external force, then fixed at 0 °C for 5 min using an ice bath. Afterwards, the temperature was raised to 80 °C, and the shape recovery behavior was recorded as the curvature radius changed at various elapsed times and temperatures during the shape recovery.

2.3 Synthesis

3-(Bis-(2-hydroxyethyl)) aminopropyltetrazole (HAPTZ)

DEA and AN were mixed in water in a molar ratio of 1:2 and stirred for 48 h at room temperature. After evaporating water and the unreacted AN, the intermediate product, 3-(bis-(2-hydroxyethyl)) aminopropanenitrile (BHAN) was obtained. Then NaN_3 and $ZnCl_2$ were added into the DMF solution of BHAN at 120 °C in a molar ratio of 4:4:1 for NaN_3:$ZnCl_2$:BHAN, and stirred for 48 h. After being cooled to 30 °C, hydrochloric acid (1 M) was dropped into the reactant, and stirred at 60 °C for another 12 h. After DMF was removed by distillation, the resultant salt was filtrated, recrystallized from methylcyanide/ether, and dried in a vacuum oven, obtaining 3-(bis-(2-hydroxyethyl)) aminopropyltetrazole, named HAPTZ, as a brown viscous liquid (yield: 79%).

Hyperbranched poly(urethane-tetrazole) (HPUTZ)

The obtained HAPTZ (0.1 mol) was firstly dissolved in anhydrous DMF at 30 °C. Then HDI (0.1 mol) was dropped into the HAPTZ solution using a dropping funnel. After reacting for 8 h, the dibutyltin dilaurate (DBTDL) (1 mL) used as a catalyst was added, and stirred for 12 h at 90 °C. Afterwards, the solution was poured into ether and washed by water. The final product, hyperbranched poly(urethane-tetrazole), named HPUTZ, was obtained as a brown solid (yield: 72%) after water was removed and dried in a vacuum oven.

Crosslinking of HPUTZ with PEG-IPDI

The semi-adduct (PEG-IPDI) was obtained from the reaction of polyethylene glycol with isophorone diisocyanate. PEG 400 (0.1 mol) reacted with IPDI (0.2 mol) in anhydrous DMF (100 mL) in the presence of DBTDL (1 mL) at 30 °C for 4 h. Then HPUTZ was mixed with PEG-IPDI according to the weight ratio as listed in Table 1, and stirred for 2 h at room temperature to form a homogeneous solution. The mixture was then cast into a Teflon mould and maintained in an oven under vacuum at 60 °C for 4 h, 80 °C for 48 h to obtain the crosslinked film, named HPUTZ-PU. Moreover, according to the weight ratios of 1:2, 1:3, and 1:4 for HPUTZ:PEG-IPDI in the formulations, the cured HPUTZ-PU1-2, HPUTZ-PU1-3, and HPUTZ-PU1-4 were obtained, respectively.

3 Results and discussion

3.1 Synthesis and characterization

The synthesis route for HPUTZ is shown in Scheme 1. The intermediate product BHAN was synthesized by the Michael addition reaction of double bond with amine group, then further cyclized with nitrile to form the 5-substituted tetrazole, HAPTZ, in the presence of a protonic acid (HCl) in DMF. In order to increase the reactivity HAPTZ further reacted with HDI to form HPUTZ as a BB'_2 type monomer through the reaction of isocyanate group with the active hydrogen atom on the tetrazole ring.

The FTIR spectra of BHAN and HAPTZ are shown in Figure 1. It can be seen that the peak at 2256 cm^{-1} in the FTIR spectrum of BHAN attributing to the stretching vibration of nitrile group disappeared completely in the FTIR spectrum of HAPTZ. However, the peak at 1665 cm^{-1} attributed to the bending vibration of tertiary amine is maintained, which is also attributed to the N-H flexural vibration of the tetrazole ring.

Figure 2 shows the ^1H NMR spectra of BHAN and HAPTZ. From the spectrum shown in Figure 2 (a), the peaks at 2.58 and 2.81 ppm attributed to the protons of nitrile propyl group (NC-CH_2-CH_2-) formed in the Michael addition reaction of DEA with AN are observed. The peak at 8.08 ppm in the spectrum of HAPTZ, as shown in Figure 2(b), is attributed to the proton of tetrazole, indicating that the cyclizative condensation of nitrile group has taken place to form HAPTZ. Moreover, four main peaks from 3.00 to 3.80 ppm attributed to the protons of methylene groups appeared, but the shifts altered due to the resonance vibration of tetrazole ring compared with that for BHAN.

Figure 3 shows the ^1H NMR spectrum of HPUTZ. The peaks at 7.09 and 5.73 ppm are attributed to the protons in amide and urethane groups formed from the reactions of isocyanate group with the active hydrogen on tetrazole ring and hydroxyl group of DEA, respectively. The peaks around

Table 1 Dynamic mechanical properties of HPUTZ-PUs

Sample	HPUTZ to PEG-IPDI (weight ratio)	T_g (°C)	E'_l $^{a)}$ (MPa)	E'_h $^{b)}$ (MPa)	E'_l $^{a)}$ / E'_h $^{b)}$	$V^{c)}$ (mol/L)
HPUTZ-PU1-2	1:2	58.9	1620	51.4	31.5	5.69
HPUTZ-PU1-3	1:3	57.7	1450	41.9	34.6	4.66
HPUTZ-PU1-4	1:4	49.8	2170	20.1	108.1	2.28

a) At the temperature of T_g −30 °C; b) at the temperature of T_g +30 °C; c) crosslinking density by DMTA.

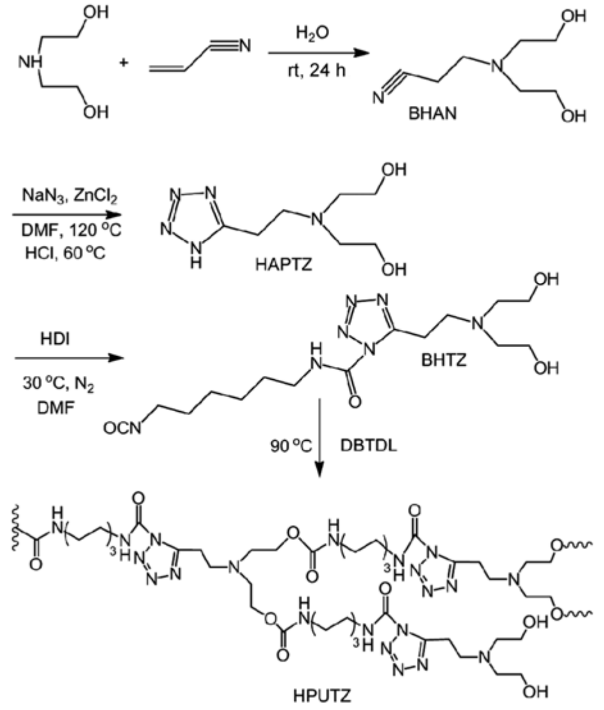

Scheme 1 Synthesis route for HPUTZ.

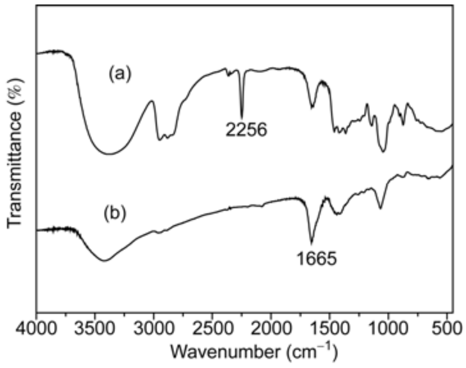

Figure 1 FTIR spectra of BHAN (a) and HAPTZ (b).

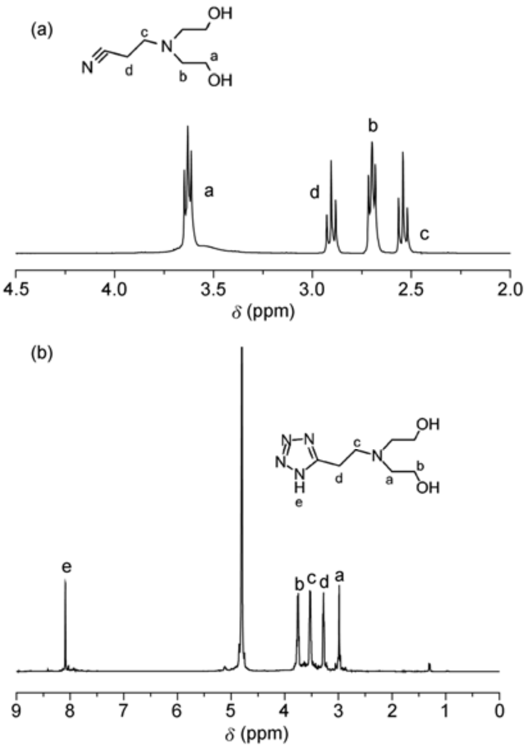

Figure 2 ^{1}H NMR spectra of BHAN in $CDCl_3$ (a) and HAPTZ in D_2O (b).

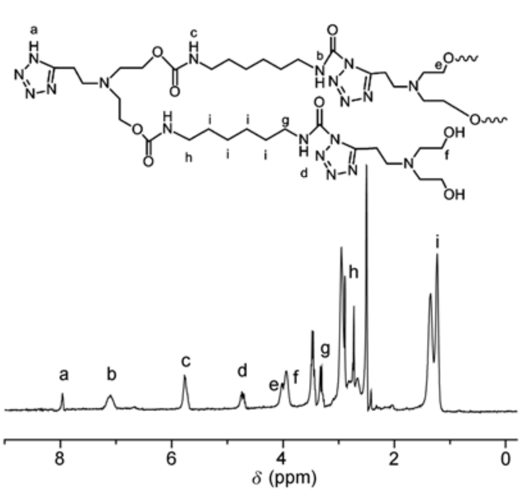

Figure 3 ^{1}H NMR spectra of HPUTZ in DMSO-d_6.

4.19 and 3.95 ppm are attributed to the protons neighbouring the ester group (–CH_2–OOC–) and hydroxyl group (–CH_2–OH), respectively. The double peaks around 1.20 ppm are assigned to the hydrogen atoms in middle methylene groups derived from hexadiisocyanate. The peak caused by the proton of tetrazole ring appears at 8.01 ppm. It is noteworthy that the peak can be also observed around 4.72 ppm, which is attributed to the proton of terminal amide group [22].

In order to determine the number average molecular weight and its distribution by GPC analysis the HPUTZ was terminated by acetate anhydride, leading to the formation of terminal ester and 1,3,4-oxadiazole. The GPC trace of HPUTZ is shown in Figure 4. The number average molecular weight (M_n) was experimentally measured to be 1.05× 10^4 g/mol. The wide molecular weight distribution of 1.27 was not only due to the high steric hindrance resulting from the dense tetrazole rings, but also the statistics of various reactions in the system. Furthermore, HPUTZ showed a bimodal distribution of molecular weight, relating to the elution volumes of 32.5 and 33.8 mL. The similar behavior has been reported for hyperbranched poly- mers [23–25].

3.2 Thermal properties

The DSC curves of HPUTZ-PUs are shown in Figure 5. It can be found that there was no crystallization area in the films, only the glass transition occurred, indicating that the microstructures of films are homogeneous [26]. There was no crystalline phase observed from the DSC curves. The

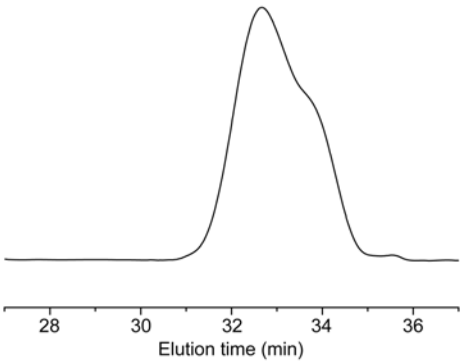

Figure 4 GPC trace of HPUTZ terminated by acetate anhydride.

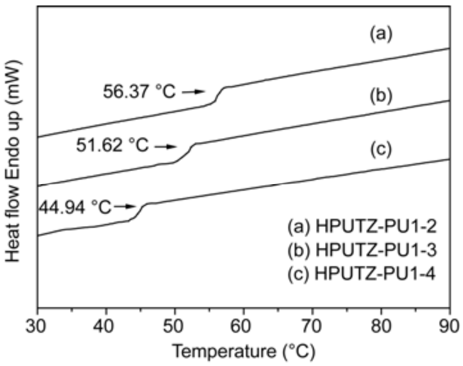

Figure 5 DSC curves of HPUTZ-PU1-2 (a), HPUTZ-PU1-3 (b) and HPUTZ-PU1-4 (c).

reason may be that the hyperbranched structure of HPUTZ restrains the crystalline course of the PEO segment. Moreover, the extensive hydrogen bond structure limits the PEO segments in order accumulation in the curing film. The similar result can be seen in ref. [26]. The DSC curves also show that T_g increased from 44.9 to 56.4 °C as the weight ratio of HPUTZ to PEG-IPDI segment content increased from 1/4 to 1/2. It can be interpreted that the tetrazole rings in HPUTZ which act as hard segments aggregate together via strong hydrogen bonding to form stable dispersed domains (frozen phase) [15]. Consequently, the increase of HPUTZ segment content resulted in the enhancement of frozen phase, and thus the increase in T_g, due to the restriction of motion of the molecular chain caused by the dense hydrogen bonding.

The effects of HPUTZ segment content on the storage modulus (E') of cured film are shown in Figure 6. It is observed that all the HPUTZ-PU films have high glassy E' values of over 1400 MPa at –40 °C as well in the glass transition process. However, the E' value of HPUTZ-PU decreases sharply as the temperature increased due to the motion of amorphous polymer chain. At the rubber state, the E' values decrease to the range of 10 to 100 MPa. This demonstrates that HPUTZ-PUs possess the typical crosslinking network character, having two glass state platforms with a higher E'_l at low temperature and a lower E'_h at high temperature (Figure 6). It has been also reported that the E'_h increased with increasing the hard segment content because of that the E'_h increased with increasing the hard segment content because of the enhancement of crosslinking density. As listed in Table 1, the higher crosslinking density of 5.69 mol/L for HPUTZ-PU1-2 was obtained compared with 2.28 mol/L for HPUTZ-PU1-4.

The tanδ curves of HPUTZ-PUs with different HPUTZ segment contents are shown in Figure 7. The loss tanδ reflects directly the movement of polymer chain. The microstructure was frozen at the glass state, showing the tanδ value almost unchanged [27]. As the temperature reached to the T_g, the movement of segment was activated completely, showing the tanδ curve changed sharply. In this study, the molecular chain movement in HPUTZ-PU1-2 with high HPUTZ segment content was limited badly. Thus, the higher temperature was required to activate the movement of PEG-IPDI segment, leading to the higher T_g of HPUTZ-PU1-2 than that of others [26]. The HPUTZ-PU1-4 sample with the highest PEG-IPDI segment content shows the most obvious viscous feature. Moreover, the peak width of tanδ curve becomes broad with increasing the PEG-IPDI segment content, indicating the more uniform network structure was obtained [26]. Therefore, the T_g measured from the tanδ curve increases with increasing the HPUTZ segment content in HPUTZ-PU. The highest T_g of 58.9 °C for HPUTZ-PU1-2 with the most HPUTZ segment content among the HPUTZ-PU films was obtained, as listed in Table 1.

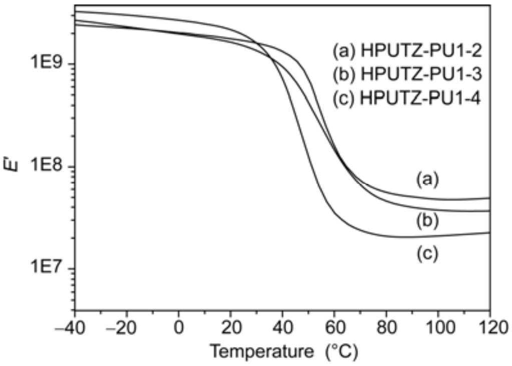

Figure 6 E' of HPUTZ-PU1-2 (a), HPUTZ-PU1-3 (b) and HPUTZ-PU1-4 (c) measured by DMTA.

3.3 Shape memory behavior

The maximum stretched length (L_max) (at the elongation of 250%), fixed length (L_F) at 0 °C, and length (L_t) in the course of shape recovery at time *t* were measured by the tension and bend deformation tests. The shape fixity (F_s) values were calculated according to the formula described in the experimental paragraph to be 90.8%, 92.7% and 93.6% at 0 °C for HPUTZ-PU1-2, HPUTZ-PU1-3 and HPUTZ-PU1-4, respectively, decreasing slightly with the increase of HPUTZ segment content directly due to the enhancement of film rigidity [15].

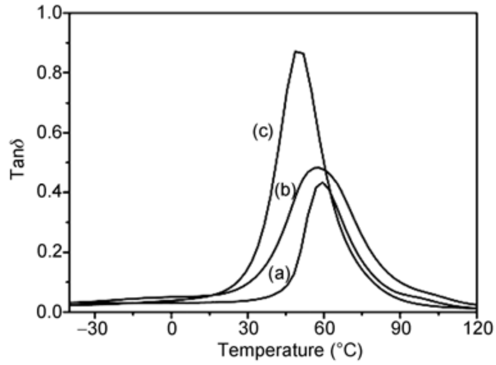

Figure 7 Tanδ of HPUTZ-PU1-2 (a), HPUTZ-PU1-3 (b) and HPUTZ-PU1-4 (c) measured by DMTA.

The shape recovery (R_s) of films obtained with different HPUTZ segment contents was calculated and plotted for the shape recovery course at 80 °C and different times, as shown in Figure 8. It is noticeable that the shape recovery rate and the time elapsed for the shape recovery are influenced sharply by the HPUTZ segment content [28–30]. Therefore, the HPUTZ-PU1-2 film with higher hard segment content shows the maximal shape recovery rate and the fastest shape recovery behavior. All the films recovered the original shape completely within 60 s at 80 °C in the tension deformation tests. The shape recovery rate was related to the stored deformation energy when the film was cooled. The enough stored deformation energy can make the film recover the original shape quickly. The HPUTZ-PU1-2 film, showing the highest storage modulus at high temperature in DMA (Table 1), possesses the most rapid shape recovery rate. Generally speaking, the shape memory polymers are required to have a small ratio of $E'_{\rm l}/E'_{\rm h}$, which is beneficial to the fixation of shape at low temperature and deformation at high temperature [26, 27]. From Table 1, the ratios of 31.5 for HPUTZ-PU1-2 and 108.1 for HPUTZ-PU1-4 were obtained. Moreover, the high $E'_{\rm h}$ at high temperature could store more deformation energy when the polymer was cooled after deformation at high temperature, which is helpful to shape recovery at a critical temperature [12–14]. As shown in Figure 9, all the films with different HPUTZ segment contents possess the excellent shape memory function at moderate temperatures, which caused by the interaction between the HPUTZ and PEG-IPDI segments. Thus, the shape recoverability can be regulated via changing the HPUTZ segment content in HPUTZ-PU.

In order to further study the shape memory property, the bend deformation tests for the circular shape films with different HPUTZ segment contents were also carried out based on the curvature radius changes at various elapsed times and temperatures during the shape recovery. The curvatures described as the reciprocal of radius were calculated and are shown in Figure 10 as the function of elapsing time. It can be seen that the shape recovery rate increases with increasing the HPUTZ segment content in HPUTZ-PU, which is the similar result with that obtained from the tension deformation test [22]. The movement of soft segment chain directly influenced the shape memory behavior of a film. The higher hard segment content leads to the improvement in the storage modulus at high temperature. Accordingly, the maximum shape recovery rate can be obtained with the highest hard segment content [31]. The shape recovery performance can be also compared by the curvatures as the function of heating temperature, as shown in Figure 11. All the results are in good agreement with that in the tension deformation tests as discussed above.

4 Conclusions

In this work, a novel hyperbranched poly(urethane-tetrazole) (HPUTZ) was synthesized via the polycondensation of an A_2 type monomer with a BB'_2 type monomer for the first time. The M_n of HPUTZ was measured to be 1.05×10^4 g/mol with a polydispersity of 1.27 by GPC analysis. The glass transition temperature of HAPTZ-PU increased from 44.9 to 56.4 °C as the HPUTZ content increased from 20% to 33% from the DSC analysis. The DMA results indicated that the HPUTZ-PU with 20% HPUTZ possessed the highest storage modulus and loss tangent. However, the storage modulus increased with the increasing of HPUTZ segment at higher temperature. The shape memory study showed that

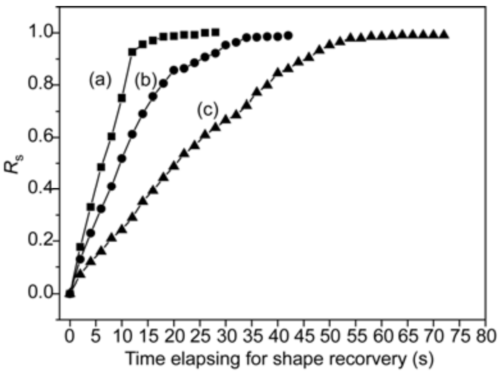

Figure 8 Strain recovery of HPUTZ-PU1-2 (a), HPUTZ-PU1-3 (b) and HPUTZ-PU1-4 (c) in the tension deformation tests.

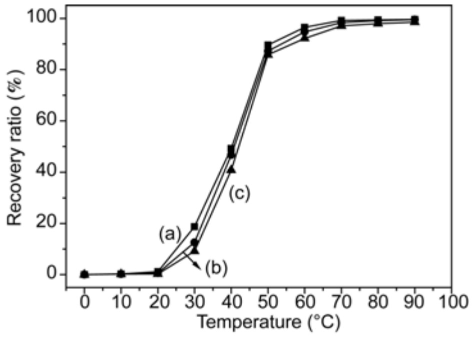

Figure 9 Strain recovery ratio of HPUTZ-PU1-2 (a), HPUTZ-PU1-3 (b) and HPUTZ-PU1-4 (c) at different temperatures for 60 s in the tension deformation tests.

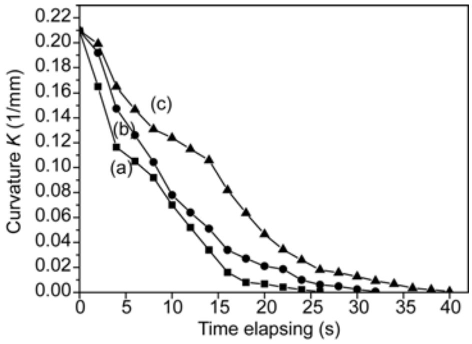

Figure 10 Time evolution of curvatures of HPUTZ-PU1-2 (a), HPUTZ-PU1-3 (b) and HPUTZ-PU1-4 (c) at 80 °C in the bend deformation tests.

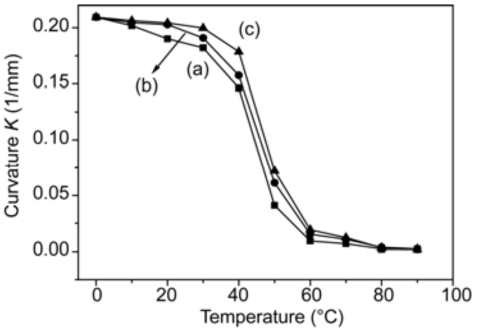

Figure 11 Curvatures of HPUTZ-PU1-2 (a), HPUTZ-PU1-3 (b) and HPUTZ-PU1-4 (c) at different temperatures for 40 s in the bend deformation tests.

all the films presented the excellent shape memory function. Over 98% shape recover could be obtained for the HAPTZ-PU with 20%–33% HAPTZ segment content within 60 s in the tension deformation test and within 40 s at 80 °C in the bend deformation test.

The financial support of the National Natural Science Foundation of China (50633010) is gratefully acknowledged.

1 Lee BS, Chun BC, Chung YC, SuI KI, Cho JW. Structure and thermomechanical properties of polyurethane block copolymers with shape memory effect. *Macromolecules*, 2001, 34(18): 6431–6437

2 Cho JW, Kim JW, Jung YC, Goo NS. Electroactive shape-memory polyurethane composites incorporating carbon nanotubes. *Macromol Rapid Commun*, 2005, 26(5): 412–416

3 Lendlein A, Kelch S. Shape-memory polymers. *Angew Chem Int Ed*, 2002, 41(12): 2034–2057

4 Wang MT, Zhang L. Recovery as a measure of oriented crystalline structure in poly(ether ester)s based on poly(ethylene oxide) and poly(ethylene terephthalate) used as shape memory polymers. *J Polym Sci Part B: Polym Phys*, 1999, 37(2): 101–112

5 Jeong HM, Lee SY, Kim BK. Shape memory polyurethane containing amorphous reversible phase. *J Mater Sci*, 2000, 35(7): 1579–1583

6 Jae HY, Byoung CC, Chan CY, Jae HC. Comparison of thermal/mechanical properties and shape memory effect of polyurethane block-copolymers with planar or bent shape of hard segment. *Polymer*, 2003, 44(11): 3251–3258

7 Tsai CC, Jen RJ. Side chain dendritic polyurethanes with shape-memory effect. *J Mater Chem*, 2009, 19: 8484–8494

8 Chen SJ, Hu JL, Yuen WC, Chan LK. Novel moisture-sensitive shape memory polyurethanes containing pyridine moieties. *Polymer*, 2009, 50(19): 4424–4428

9 Brukley CP, Prisacariu C, Caraculacu A. Novel triol-crosslinked polyurethanes and their thermorheological characterization as shape-memory materials. *Polymer*, 2007, 48(5): 1388–1396

10 D'hollander S, Assche GV, Mele BV, Prez FD. Novel synthetic strategy toward shape memory polyurethanes with a well-defined switching temperature. *Polymer*, 2009, 50(19): 4447–4454

11 Gunes IS, Cao F, Jana SC. Evaluation of nanoparticulate fillers for development of shape memory polyurethane nanocomposites. *Polymer*, 2008, 49(9): 2223–2234

12 Lendlein A, Langer R. Biodegradable, elastic shape-memory polymers for potential biomedical applications. *Science*, 2002, 296: 1673

13 Zhu G, Liang G, Xu Q, Yu Q. Shape-memory effects of radiation crosslinked poly(epsilon-caprolactone). *J Appl Polym Sci*, 2003, 90(6): 1589–1595

14 Lendlein A, Schmidt AM, Schroeter M, Langer R. Shape-memory polymer networks from oligo(epsilon-caprolactone)dimethacrylates. *J Polym Sci Part A: Polym Chem*, 2005, 43(7): 1369–1381

15 Cao Q, Liu PS. Structure and mechanical properties of shape memory polyurethane based on hyperbranched polyesters. *Polymer Bulletin*, 2006, 57: 889–899

16 Sivakumar C, Nasar AS. Poly(epsilon-caprolactone)-based hyperbranched polyurethanes prepared via A(2) + B-3 approach and its shape-memory behavior. *Eur Polym J*, 2009, 45(8): 2329–2337

17 Hickner MA, Ghassemi H, Kim YS, McGrath EJE. Alternative polymer systems for proton exchange membranes (PEMs). *Chem Rev*, 2004, 104: 4587

18 Lavrenova LG, Larionov SV. Spin transition in iron (II) complexes with 1,2,4-triazoles and tetrazoles. *Russ J Coord Chem*, 1998, 24: 379–395

19 Nicolay VT, Bernaerts KV, Dufour B, Perez FED, Matyjaszewski K. Well-defined (Co) polymers with 5-vinyltetrazole unites via combination of atom transfer radical (co)polymerization of acrylonitrile and "Click Chemistry"-type postpolymerization modification. *Macromolecules*, 2004, 37: 9308

20 Levchik SV, Balabanovich AI, Ivashkevich OA, Gaponik PN, Thermal decomposition of tetrazole-containing polymer. V. Poly-1-vinyl-5-aminotetrazole. *Polym Degrad Stab*, 1995, 47: 333–338

21 Celik SÜ, Bozkurt A, Preparation and proton conductivity of acid-doped 5-aminotetrazole functional poly(glycidyl methacrylate). *Eur Polym J*, 2008, 44: 213–218

22 Ji FL, Hu JL, Li TC, Wong YW. Morphology and shape memory effect of segmented polyurethanes. I. With crystalline reversible phase. *Polymer*, 2007, 48(17): 5133–5145

23 Shi WF, Rånby B. Photopolymerization of dendritic methacrylated polyesters. 1. Synthesis and properties. *J Appl Polym Sci*, 1996, 59(12): 1937–1945

24 Kou HG, Asif A, Shi WF, Jiang ZG, Huang WHA novel hyperbranched polyester acrylate used for microfabrications. *Polym Adv Technol*, 2004, 15: 192–196

25 Zhang Y, Fu Q, Shi WF. Synthesis and intrinsic blue fluorescence study of hyperbranched poly(ester-amide-ether). *Sci China Chem*, 2010, 53(12): 2452–2460

26 Xu JW, Shi WF, Pang WM. Synthesis and shape memory effects of Si-O-Si cross-linked hybrid polyurethanes. *Polymer*, 2006, 47(1): 457–465

27 Jeong HM, Ahn BH, Kim BK. Temperature sensitive water vapour permeability and shape memory effect of polyurethane with crystalline reversible phase and hydrophilic segments. *Polym Int*, 2000, 49(12): 1714–1721

28 Voit B. Hyperbranched polymers—All problems solved after 15 years of research? *J Polym Sci Part A: Polym Chem*, 2005, 43(13): 2679–2699

29 Gao C, Yan DY. Hyperbranched polymers: From synthesis to applications. *Prog Polym Sci*, 2004, 29(3): 183–275

30 Spindler R, Fréchet J. Macromolecules, Synthesis and characterization of hyperbranched polyurethanes prepared from blocked isocyanate monomers by step-growth polymerization. 1993, 26(18): 4809–4813

31 Cao Q, Chen SJ, Hu JL, Liu PS. Study on the liquefied-MDI-based shape memory polyurethanes. *J Appl Polym Sci*, 2007, 106(2): 993–1000